

一些多层夹心配合物的电子结构和成键

朱龙根

(南京大学配位化学国家重点实验室, 南京 210093)

Walter Siebert Hubert Wadepohl

(海得堡大学, 德国 69120)

本文采用 Fenske-Hall 方法研究了三层和四层夹心配合物的电子结构和成键。结果指出, 三层夹心配合物的稳定电子组态为 30-34 价电子(VE), 但是当金属-金属间距缩短时, 由两个过渡金属的 d_z^2 , $d_{x^2-y^2}$ 和 d_{xy} 组成的三个 MO 能级上升且定位在前线轨道区域, 因此预料 26-28VE 也是稳定电子组态。基于 MO 分析, 42VE 的四层夹心配合物是稳定电子组态, 然而由于 HOMO (d_z^2) 与 LUMO(简并轨道 d_{xy} , d_{xz}) 的能隙不大, 最大价电子数为 46 的这类化合物也可稳定存在。从 MO 图得知, 四层夹心配合物的前线轨道是由过渡金属的 5 根 d 轨道所组成, 因此预料可以制备出价电子数从 36VE 变化到 46VE 的这类化合物。根据 MO 图和微扰理论, 配合物 $[(\eta^5-C_5H_5)Fe(\mu, \eta^5-C_3B_2H_3)Co(\eta^5-C_5H_5)]^+$ 和 $[(\eta^5-C_5H_5)Fe(\mu, \eta^5-C_3B_2H_3)Fe(\eta^5-C_5H_5)]$ 的 EPR 给予了合理的解释。

关键词: 多层夹心配合物 MO EPR

ELECTRONIC STRUCTURE AND BONDING OF SOME OLIGODECKER SANDWICH COMPLEXES

Zhu Longgen^{a)} Walter Siebert^{b)} Hubert Wadepohl^{b)}

(State Key Laboratory of Coordination Chemistry, Nanjing University, Nanjing 210093, People's Republic of China^{a)} and Inorganic Chemistry Institute, University of Heidelberg, Im Neuenheimer Feld 270, 69120 Heidelberg, Federal Republic of Germany^{b)})

The electronic structure and bonding of triple-decker and tetradecker sandwich complexes have been studied by the Fenske-Hall method. The results show that the stable electronic configurations of triple-decker complexes have 30 to 34 VE, first calculated by R. Hoffmann. However, the configurations with 26 to 29 VE are also stable as the M-M distance is shortened. The energy levels of three d orbitals made up of d_z^2 , $d_{x^2-y^2}$ and d_{xy} orbitals of the two transition metals are raised and located in the frontier region. Based on a MO analysis, tetradecker complexes with 42 VE have a stable electronic configuration. However, because the splitting energy between HOMO(d_z^2 orbital) and

1. Received date 1994-11-22.

2. This work was supported by National Natural Science Foundation.

3. Zhu Longgen, male, age of 55, professor, mainly work on theoretical coordination chemistry and bioinorganic chemistry.

LUMO (degenerate orbitals d_{xy} , d_{xz}) is not large, complexes with 46 VE, which represents the maximum number of valence electrons for this series, are also stable. Because the frontier orbitals of the tetradecker complexes are made up of five d orbitals of the transition metals, a series of trinuclear complexes with 36 VE to 46 VE is expected. In the light of MO diagrams and perturbation theory, the EPR of the complexes $[(\eta^5\text{-C}_5\text{H}_5)\text{Fe}(\mu,\eta^5\text{-C}_3\text{B}_2\text{H}_5)\text{Co}(\eta^5\text{-C}_5\text{H}_5)]^+$ and $[(\eta^5\text{-C}_5\text{H}_5)\text{Fe}(\mu,\eta^5\text{-C}_3\text{B}_2\text{H}_5)\text{Fe}(\eta^5\text{-C}_5\text{H}_5)]$ can be reasonably explained.

Keywords: tripledecker tetradecker MO calculations EPR

Introduction

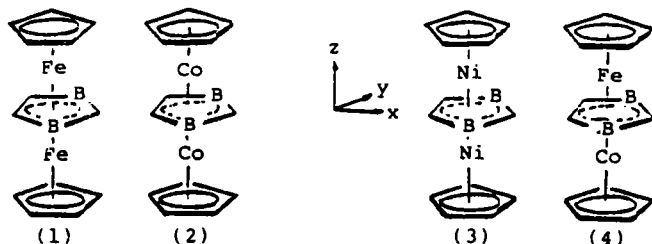
The oligo- and polydecker sandwich complexes of transition metals have attracted particular interest both synthetically and theoretically. The first complex of this type was prepared by Werner and Salzer in 1972⁽¹⁾. Further development of this field was mainly connected with the use of boron-containing heterocyclic ligands, which form triple-decker, tetradecker, and oligodecker up to decadecker complexes^(2,3). In 1976 J.W.Lauher, R. Hoffmann et al. published the results of an extended Hückel molecular orbital calculation from which two series of stable structures, containing 30 and 34 valence electrons, respectively, were predicted⁽⁴⁾. Since then, several theoretical studies on the triple-decker^(3a,5a-D) and tetradecker sandwich complexes^(5g-i) have been published.

We present here MO calculations of triple-decker and tetradecker sandwich complexes with actual structures using the Fenske-Hall method. Our study mainly focuses on electronic structure, bonding and the explanation of EPR spectra.

Results and Discussion

Triple-Decker Sandwich Complexes

Triple-decker sandwich complexes FeFe(1), CoCo(2), NiNi(3) and FeCo(4) with the 2,3-dihydro-1,3-diborolyl ligand in the bridging position were employed in our calculations.

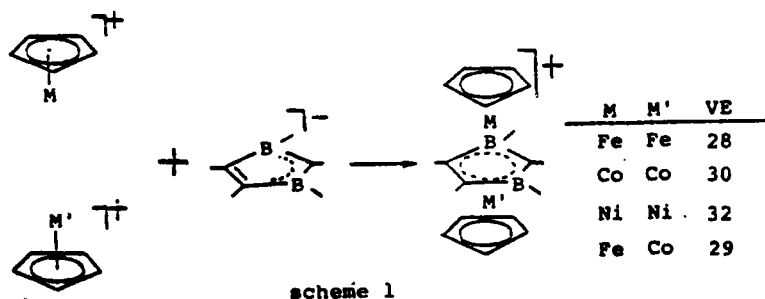


formula 1-4

1. The fragment analysis of $[\text{M}(\text{C}_5\text{H}_5)]^+$ and $(\text{C}_3\text{B}_2\text{H}_5)^-$

The electronic structure of the triple-decker sandwich complexes $[(\eta^5\text{-C}_5\text{H}_5)\text{M}(\mu,\eta^5\text{-C}_3\text{B}_2\text{H}_5)\text{M}'(\eta^5\text{-C}_5\text{H}_5)]$ may be approached from different viewpoints as pointed out by R.Hoffmann et al.⁽⁴⁾. It is convenient to divide the molecules into three fragments, as shown

schematically below.



The characteristic features of the $[M(C_5H_5)]^+$ fragment are summarized in Fig. 1.

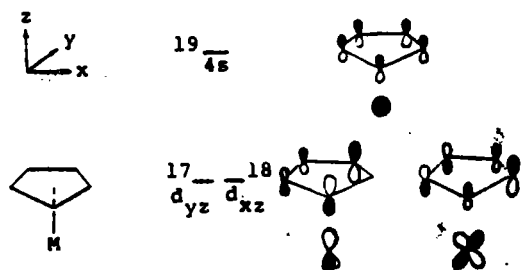


Fig. 1 Frontier orbitals of the $[M(C_5H_5)]^+$ fragment

We assume that all triple-decker complexes considered belong to the C_s point group with the symmetry plane xz . The π molecular orbitals of the $(C_3B_2H_5)$ fragment are given in Fig. 2.

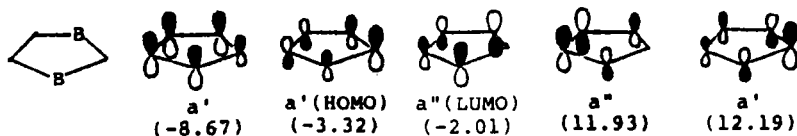
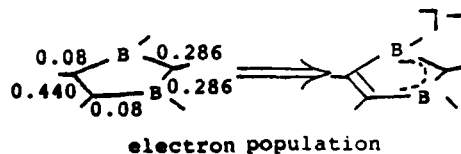


Fig. 2 π orbitals of the $C_3B_2H_5^-$ fragment

Numbers in parentheses represent MO energies in eV.

Unlike the $(C_5H_5)^-$ ring, four π electrons in the 2,3-dihydro-1,3-diborolyl ring are localized, as follows from the π electron population. Two π electrons form the C-C bond, and the two others form a three-center two-electron bond (B-C-B). Since the LUMO of the $C_3B_2H_5^-$ ring is at low energy and has bonding character between boron and carbon (of the C-C bond) it can easily accept two electrons, resulting in aromaticity of the $(C_3B_2H_5)^{3-}$ ring, just



like $(C_5H_5)^-$. But it should be emphasized that there is a difference in the bonding of the $(C_3B_2H_5)^-$ and $(C_5H_5)^-$ rings to the $[M(C_5H_5)]^+$ fragment. The $(C_3B_2H_5)^-$ ring is taken as a do-

nor / acceptor for bonding, the $(C_3H_3)^-$ ring as a donor in $[(C_3H_3)M(\mu-C_3H_3)M'(C_3H_3)]^+$ ($M, M' = Ni$ and Fe for $\mu-C_3H_3$)⁽⁶⁾.

2. Interaction between the fragments

MO diagrams for interactions of the three fragments are given in Fig.3 and Fig.4. On the right of Fig.3 and Fig.4 are shown the π orbitals of the bridging ligand $(C_3B_2H_3)^-$, designated to a' , a' and a'' , respectively. These fragment orbitals interact strongly with the corresponding symmetry combinations derived from the $[M(C_3H_3)]^+$ $4s, 3d_{xz}, 3d_{yz}$ orbitals. Our calculations also show that there are important interactions of the σ orbitals of the $(C_3B_2H_3)^-$ and $(C_3H_3)^-$ rings with appropriate symmetry orbitals of the metal atoms. These interactions affect the energy levels of the d_{xz} and d_{yz} orbitals (HOMOs in 3 and LUMOs in 1). These orbitals were assigned essentially as non-bonding in the early calculations of $Ni_2Cp_3^+$ ⁽⁴⁾. Since the distances between M and M' become shorter from $NiNi$ (3.42 Å), through $CoCo$ (3.28 Å), to $FeFe$ (3.17 Å), the energies of the d_{xz} and d_{yz} orbitals increase from the $NiNi$ to the $FeFe$ complex.

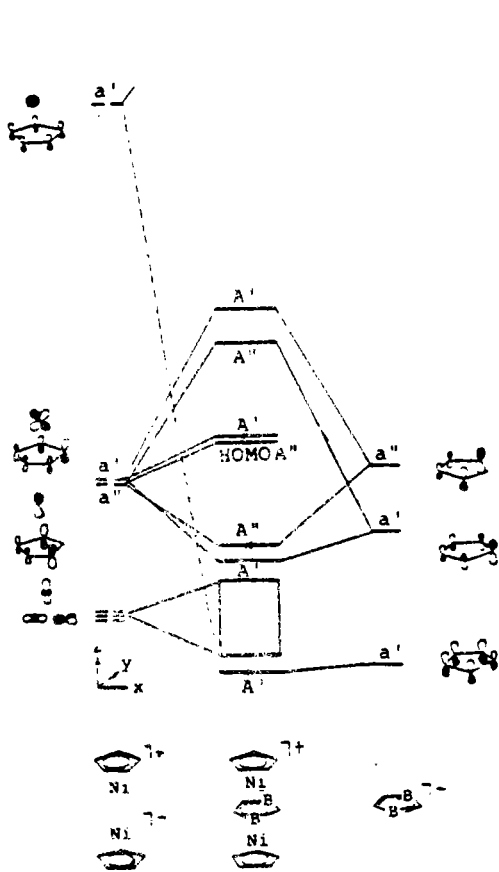


Fig 3 MO diagram of 3

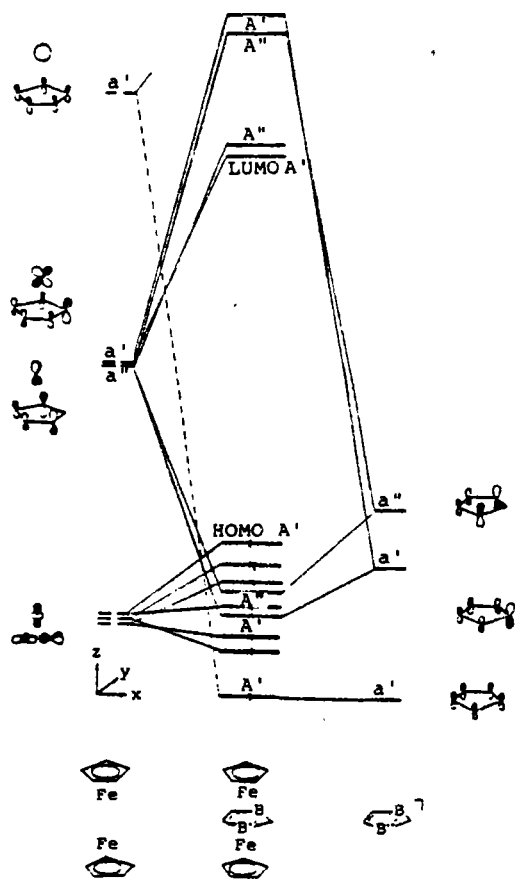
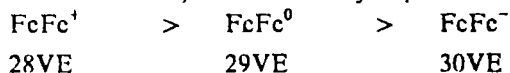


Fig.4 MO diagram of 1

The d_{xz} and d_{yz} orbitals in the $NiNi$ complex (Fig.3) are at slightly higher energy than the

corresponding fragment orbitals of the $[\text{Ni}(\text{C}_5\text{H}_5)]^+$ fragments. Thus it can be predicted that the anionic NiNi complexes (3^-) with 34 VE are stable as was found experimentally^(3a). Because of the σ -antibonding character of the d_{xz} and d_{yz} orbitals, the triple-decker complexes with 30 VE should be more stable than those with 31 to 34 VE. The same conclusion was obtained by R. Hoffmann et al. for Ni_2Cp_3^+ . The d_{xz} and d_{yz} orbitals in the CoCo^+ complex (2^+) are higher than those in the NiNi^+ complex. The energy gap between HOMO and LUMO may not allow to fill in four electrons in the LUMO to obtain the triple-decker $(\text{CoCo})^{3-}$ with 34 VE. Based on the same reasoning it would be impossible to generate the 31 VE triple-decker complex FeFe^{2-} . This was confirmed by electrochemical studies^(3c). Comparing the MO diagrams of these triple-decker complexes, the results are noteworthy. A striking difference between FeFe^+ and NiNi^+ , CoCo^+ complexes is observed. The HOMO of CoCo^+ and NiNi^{3+} with 30 VE represent bonding orbitals of two fragments, d_{yz} of $\text{M}(\text{C}_5\text{H}_5)^+$ (a'') and the low-lying vacant orbital of $(\text{C}_3\text{B}_2\text{H}_3)^-$. The HOMO-1 orbital is also bonding between d_{xz} (a') and the high-lying occupied orbital of $(\text{C}_3\text{B}_2\text{H}_3)^-$ (a'). The six d -block orbitals are located below these two orbitals. It is evident that NiNi^{4+} (29 VE) and CoCo^{2+} (29 VE) would be difficult to obtain (compare ref. 3a). In contrast to this, the HOMO of the FeFe complex (1) is mainly attributed to d_z orbitals of both iron atoms and has some antibonding character. In addition the orbital next to the HOMO is also of interest because it is mainly composed of the d_{xy} orbitals of the two $\text{Fe}(\text{C}_5\text{H}_5)^+$ fragments. HOMO and HOMO-1 are very close to each other with an energy difference of about $62.8\text{kJ} \cdot \text{mol}^{-1}$.

The small energy difference is in good agreement with the weak temperature-dependent paramagnetism, which was observed experimentally for the 28 VE FeFe^+ complex^(3d). It would be anticipated that removing an electron from the HOMO of the FeFe^0 complex should make the complex more stable, i.e. the stability sequence of FeFe complexes should be as follows:



Indeed, the overlap population between d_z orbitals shows that the small antibonding interaction ($-0.02e$ for FeFe^-) is changed into small bonding interaction ($0.03e$ for FeFe , $0.07e$ for FeFe^+) when the number of valence electrons is changed from 30 VE to 28 VE. The energy of the d_{xz-yz} orbital is higher than that of the strongly bonding combination of the two fragment d_{yz} orbitals (a'') and the low-lying vacant orbital of $(\text{C}_3\text{B}_2\text{H}_3)^-$ (a''). Therefore the highest three occupied levels in FeFe -like complexes are expected to fall within a very narrow energy range. It is possible for the complexes with electron numbers ranging between 26 and 29 to have interesting magnetic properties. From EPR data of FeFe (29 VE), however, it should be mentioned that we find a nondegenerate d_{xy} ground state for the neutral complex (see below). This requires the ordering of the HOMO (d_z) and orbital next to it (d_{xy}) levels in our calculation to be reversed. Since the computed energy difference between these levels is, as mentioned above, very small, this is not a serious discrepancy considering the approximate method used in our calculation (see below). For the 29 VE complex FeCo^+ the HOMO is mainly attributed to d_z orbital

of iron. In other words, an unpaired electron is mostly localized on the iron atom. The orbital next to the HOMO is the strongly bonding combination of the d_{yz} orbitals of $\text{Fe}(\text{C}_5\text{H}_5)^+$, $\text{Co}(\text{C}_5\text{H}_5)^+$ and the low-lying vacant orbital of $(\text{C}_3\text{B}_2\text{H}_5)^-$. The LUMOs (degenerate orbitals A' and A'') are mainly composed of the d_{xz} and d_{yz} , respectively, of Co, with small contributions from the d_{xz} and d_{yz} , respectively, of the iron atom.

3. Comparison of the stability of triple-decker complexes

In the Table 1 and Table 2 the total overlap populations are presented which allow to compare the bonding between $\text{M}(\text{C}_5\text{H}_5)^+$ ($\text{M} = \text{Fe}, \text{Co}$ and Ni) and the $(\text{C}_3\text{B}_2\text{H}_5)^-$ ring and between M and the $(\text{C}_5\text{H}_5)^-$ ring.

Table 1 Total Overlap Populations between CpM and the $(\text{C}_3\text{B}_2\text{H}_5)^-$ ring (in e)

complex	VE	C2	B1	B3	C4	C5
FeFe^-	30	0.186	0.159	0.159	0.140	0.140
FeFe	29	0.209	0.170	0.170	0.153	0.153
FeFe^+	28	0.232	0.179	0.179	0.160	0.160
CoCo^+	30	0.139	0.113	0.113	0.093	0.093
NiNi^+	32	0.053	0.054	0.054	0.061	0.061

Table 2 Total Overlap Populations between M and the Cp ring (in e)

complex	VE	C2	C1	C3	C4	C5
FeFe^-	30	0.107	0.093	0.093	0.088	0.088
FeFe	29	0.128	0.116	0.116	0.108	0.108
FeFe^+	28	0.152	0.139	0.139	0.128	0.128
CoCo^+	30	0.106	0.091	0.091	0.082	0.082
NiNi^+	32	0.013	0.056	0.056	0.024	0.024

It can be clearly seen from Table 1 that the total overlap population in the 28VE complex FeFe^+ is larger than that of 29VE complex FeFe^0 , which is larger than that of the 30VE complex FeFe^- . These results further confirm the conclusion obtained by the analysis of the MO diagram.

Comparing the data for FeFe^n ($n = +1, 0, -1$) with the CoCo^+ and NiNi^+ complexes, it appears that the bonding in the 30 VE complex CoCo^+ is not as strong as that in the 30 VE complex FeFe^- . Weakest covalent interactions are found in the 32 VE complex NiNi^+ . The data in Table 2 also show that the bonding interaction between the transition metals and the $(\text{C}_5\text{H}_5)^-$ rings is the best for iron, intermediate for cobalt and worst for nickel.

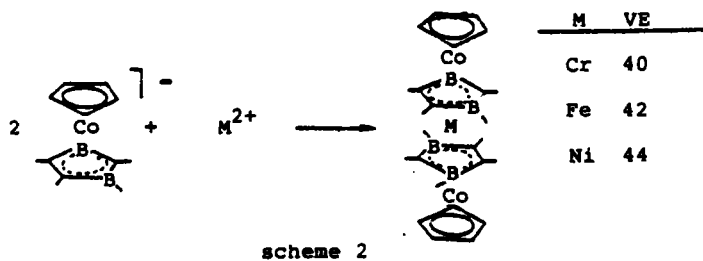
Tetradeccker Sandwich Complexes

The tetradeccker sandwich complexes $[(\eta^5-\text{C}_5\text{H}_5)\text{Co}(\mu, \eta^5-\text{C}_3\text{B}_2\text{R}_5)]_2\text{M}$ ($\text{M} = \text{Cr}, \text{Mn}, \text{Fe}, \text{Co}, \text{Ni}, \text{Cu}$ and Zn) have been synthesized^(3b). We take three tetradeccker sandwich complexes $[(\eta^5-\text{C}_5\text{H}_5)\text{Co}(\mu, \eta^5-\text{C}_3\text{B}_2\text{H}_5)]_2\text{M}$ ($\text{M} = \text{Cr}, \text{Fe}$ and Ni) as examples to discuss the general findings of the series. The structures of the complexes chosen for calculation are taken from X-ray data⁽¹⁰⁾.

1. The fragment analysis of $[(\eta^5-\text{C}_5\text{H}_5)\text{Co}(\eta^5-\text{C}_3\text{B}_2\text{H}_5)]^-$

Experiments show that two molecules of the sandwich anion $[(\eta^5-\text{C}_5\text{H}_5)\text{Co}(\eta^5-\text{C}_3\text{B}_2\text{R}_5)]^-$ react with one metal ion M^{2+} to form the tetradeccker sandwich complexes

$[(\eta^5-C_5H_5)Co(\mu,\eta^5-C_3B_2R_3)]_2M$. Therefore, it is convenient to divide the trinuclear molecule into three fragments, as shown schematically below.



The sandwich anion $[(\eta^5-C_5H_5)Co(\eta^5-C_3B_2H_3)]^-$ is divided, in turn, into fragments of $M(C_5H_5)^0$ and $(C_3B_2H_3)^-$. The characteristic features of the $M(C_5H_5)^0$ and $(C_3B_2H_3)^-$ fragments have been discussed in the previous section. The MO diagram of the $[(\eta^5-C_5H_5)Co(\eta^5-C_3B_2H_3)]^-$ fragment is given in Fig. 5. We assume that the fragment

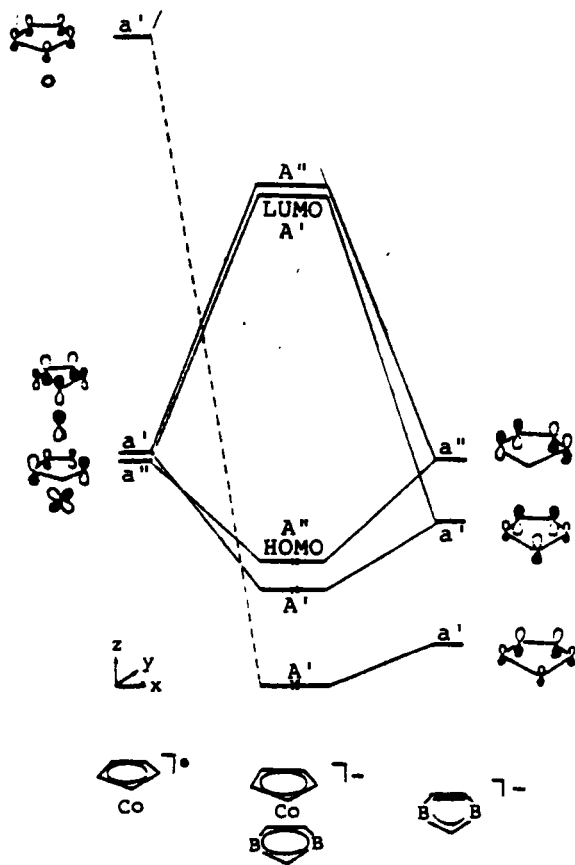
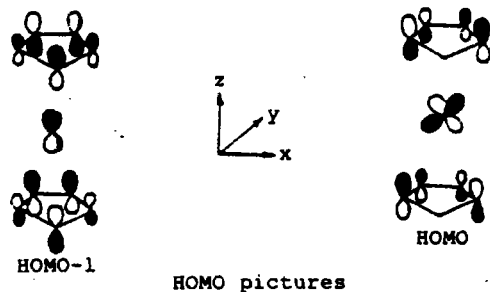


Fig.5 MO diagram of $[(\eta^5-C_5H_5)Co(\eta^5-C_3B_2H_3)]^-$

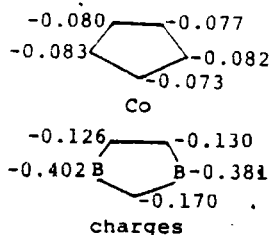
$[(\eta^5-C_5H_5)Co(\eta^5-C_3B_2H_3)]^-$ has C_s symmetry with the symmetry plane yz . On the right are presented the frontier orbitals of the $(C_3B_2H_3)^-$ fragment, which interact with frontier orbitals of corresponding symmetry of the $M(C_5H_5)^0$ fragment, resulting in three bonding molecular

orbitals. It is clearly seen from Fig.5 that the HOMO of A'' symmetries is a strongly bonding orbital, and the LUMO designated as A' is a strongly antibonding one. The energy gap between HOMO and LUMO is very large. It thus is expected that the sandwich anion $[(\eta^5-C_3H_5)Co(\eta^5-C_3B_2H_5)]^-$ with 18 VE is quite stable.

The bonding character of the HOMO and the orbital next to the HOMO is pictured as follows:



These two orbitals are responsible for the bonding of the $[(\eta^5-C_3H_5)Co(\eta^5-C_3B_2H_5)]^-$ anion with the d orbitals of the metal ions. Another notable feature of the fragment is the distribution of the electric charge. Unlike the $(C_3H_5)^-$ ring, the fragment $(C_3B_2H_5)^-$ has a capacity of accepting electrons when bonding to the $Co(C_3H_5)$ fragment. As a result, a higher negative charge is localized on the $(C_3B_2H_5)^-$ ring, as shown



The total negative charge on the $(C_3B_2H_5)^-$ ring is about 1.2e. Hence, the boron heterocycle in the sandwich anion may be regarded as a hard base when it interacts with metal ions. Therefore covalent bonding between two $[(\eta^5-C_3H_5)Co(\eta^5-C_3B_2H_5)]^-$ fragments and M^{2+} is realized by orbital interaction, while ionic bonding may also exist through electrostatic interaction.

2. Orbital interactions between two fragments $[(\eta^5-C_3H_5)Co(\eta^5-C_3B_2H_5)]^-$ and metal ions M^{2+}

Calculations were carried out on three tetradecker complexes $[(\eta^5-C_3H_5)Co(\mu, \eta^5-C_3B_2H_5)]_2M$ ($M = Cr, Fe$ and Ni) as representatives. The MO diagram for the Cr complex is shown in Fig.6.

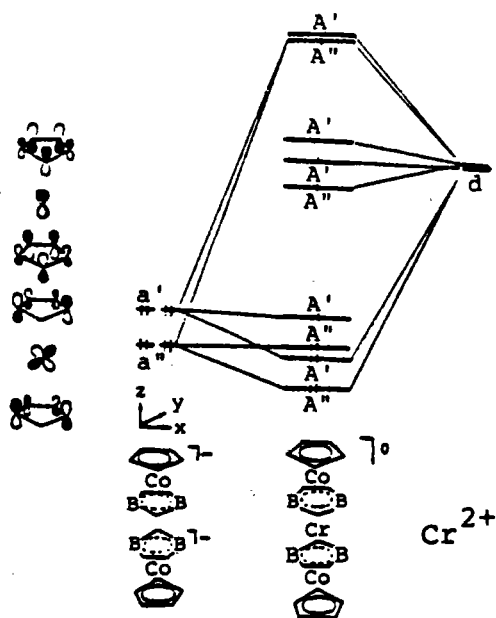
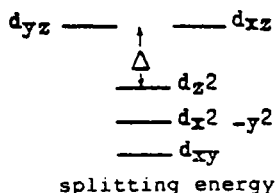


Fig.6 MO diagram of $[(\eta^5-C_3H_5)Co(\mu, \eta^5-C_3B_2H_5)]_2 Cr$

The corresponding diagrams of the iron and nickel complexes (CoFcCo and CoNiCo) are quite similar. Bonding (A'' and A'), nonbonding (A'' and A') and antibonding (A'' and A') orbitals are generated by interaction of two a'' fragment orbitals of $[(\eta^5-C_3H_5)Co(\eta^5-C_3B_2H_5)]^-$ with d_{xz} of M^{2+} , and two a' fragment orbitals of $[(\eta^5-C_3H_5)Co(\eta^5-C_3B_2H_5)]^-$ with d_{yz} of M^{2+} . The frontier orbitals are mainly composed of five d orbitals of M^{2+} . The degenerate low-lying antibonding orbitals (mainly d_{yz} and d_{xz}) have some contribution from the fragment orbitals of the two $[(\eta^5-C_3H_5)Co(\eta^5-C_3B_2H_5)]^-$ fragments. As obvious from Fig.6 the number of valence electrons in the series can be varied from 36 to 46. The tetradecker complexes with 42 VE where the antibonding orbitals (d_{yz} and d_{xz}) are empty will be preferred. It is anticipated that the complexes with less than 40 VE, such as $M = Sc(d^1), Sc(d^2), Ti(d^2), Ti(d^3), V(d^2), V(d^3)$ etc., could also be prepared. The bonding picture is just like the splitting of the five d orbitals of transition metal ions in a ligand field. The splitting energy of the ligand field, Δ , corresponds to the energy difference between the d_z^2 orbital and the low-lying antibonding orbitals, d_{xz} and d_{yz} , as shown below.



The Δ values decrease going from Cr through Fc to Ni. Low-spin and high-spin tetradecker complexes will be anticipated, depending on the splitting energy Δ . The magnetic data show that $[(\eta^5-C_3H_5)Co(\mu, \eta^5-C_3B_2R_3)]_2 Cr (d^4)$ is high-spin state with $\mu_{eff} = 4.70(5)$ B.M.; the Fc(d^4) complex is also high-spin ($\mu_{eff} = 4.94(4)$ B.M.), but its cation is low-spin with

$\mu_{\text{eff.}} = 2.74(5)$ B.M. ^(7,10). The Ni(d^8) complex is also paramagnetic ⁽⁷⁾. It should be mentioned that the Δ values calculated in the MO diagrams are incorrect in absolute sense. However, these values can be used for comparison in the series. For instance, the value calculated for the Cr(d^4) complex is 2.79 eV, which results in a high-spin state. As expected, the Fe(d^6) complex should also be high-spin as the Δ value for this complex is 2.51 eV. However, the Δ value for the Fe(d^5) complex (CoFeCo)⁺ is about 2 eV higher than that of the Fe(d^6) complex (CoFeCo). Therefore the (CoFeCo)⁺ has a low-spin state, as confirmed experimentally. In the Ni(d^8) complex, the three lower d orbitals are occupied by six electrons, and the degenerated orbitals, separated by Δ , have one electron each. Therefore it can be assumed that the arrangement of the frontier orbitals given in Fig.6 is qualitatively correct. The observed magnetic data of the tetradeccker sandwich complexes are well accounted by our MO diagrams.

Interpretation of EPR Data of The Triple-Decker Complexes FeCo⁺ and FeFe

As stated above the unpaired electron in the 29 VE complex FeCo⁺ is principally localized on the Fe atom ^(3a). This complex may thus be treated as a ferricenium analogue. However, comparing g values of this complex with those of ferricenium ions and their analogues ^(8b), it is found that they are quite different. This difference in g values can be interpreted by MO diagrams. The ground state of the ferricenium ion is the orbitally degenerate $(a_{1g})^2(e_{2g}^{\pm})^3$ configuration.

The large deviation of the g values from 2.0023 in ferricenium ion indicates that the orbital momentum contribution to the g values is large ⁽⁸⁾. Our MO diagram of the 29 VE complex FeCo⁺ shows that the HOMO is mainly composed of the d_{z^2} orbital of the iron atom. In this case, the g values are expected to be close to 2, which is in good agreement with the observed value of 2.11 ^(3a).

The similarity of the ESR spectra of FeFe ^(3c) to ferricenium and the carborane ferricenium analogues ⁽⁸⁾ has prompted us to use the ground state configuration of $(a_{1g})^2(e_{2g}^{\pm})^3$ ($a_{1g} = d_{z^2}$, $e_{2g}^+ = d_{xy}$, $e_{2g}^- = d_{x^2-y^2}$), based on D_{5d} symmetry, as starting point. Following Maki and Berry's treatment ^(8a), we assume, that the ground state, ${}^2E_{2g}$, is split into two Kramer's doublets by spin-orbit-coupling and crystal fields of lower symmetry than D_5 .

Wave functions and energies for the lower ($\Psi_{\pm}^{(a)}$) and upper ($\Psi_{\pm}^{(b)}$) doublets are given in ref.[8a]. The resulting g -values are given by equations (1) and (2) ^(8a).

$$\begin{vmatrix} \xi - W & \delta \\ \delta & -\xi - W \end{vmatrix} = 0$$

$$\Psi_{\pm}^{(a)} = \begin{cases} N(e_{2g}^+ + \zeta e_{2g}^-)\alpha \\ N(e_{2g}^- + \zeta e_{2g}^+)\beta \end{cases} \quad W^{(a)} = -(\xi^2 + \delta^2)^{1/2} \tag{1}$$

$$\Psi_{\pm}^{(b)} = \begin{cases} N(e_{2g}^- - \zeta e_{2g}^+)\alpha \\ N(e_{2g}^+ - \zeta e_{2g}^-)\beta \end{cases} \quad W^{(b)} = +(\xi^2 + \delta^2)^{1/2} \tag{2}$$

ζ is the effective spin-orbit coupling parameter, k' the orbital reduction parameter.

Using the one-electron spin-orbit coupling constant ξ_0 of the free Fe^{3+} ion (440 cm^{-1})⁽⁹⁾, $\xi \approx 0.793$, and $k' \approx 1.0$ are obtained by fitting the equations (1) and (2) to the experimental values^(3c) for g_{\parallel} (≈ 2.91) and g_{\perp} (≈ 1.97).

The splitting energy of d_{xy} and $d_{x^2-y^2}$, Δ , is estimated to be 4231 cm^{-1} (0.524 eV). This value compares favourably to the calculated energy difference between the HOMO and the orbital next to HOMO (0.40 eV). As pointed out in ref.[8], the g factor derived from the alternative ground state configuration of $(e_{2g}^+)^4(a_{1g})^1$ is expected to be nearly isotropic and close to 2 because of the absence of a low-symmetry crystal field perturbation.

Details of the Calculations

An approximation to the Hartree-Fock Roothaan technique, the Fenske-Hall method, has been described elsewhere⁽¹¹⁾. This iterative SCF method is devoid of empirical or adjustable parameters, so that results of a calculation—eigenvalues, eigenvectors and derived quantities—are determined fully by the molecular geometry and by the basis functions. The small but significant effects of the intramolecular electrostatic interactions are taken into account in the computation of the Fock matrix elements. Consequently, the energies of the fragment orbitals (diagonal elements in the Fock matrix) reflect the influences of the molecular environment on the fragments "ready for bonding" and the energies of the molecular orbitals depend somewhat on the overall distribution of charges in a molecule. Each molecule or a larger fragment was divided into two subfragments bearing chemically meaningful charges. The transformations of basis sets and partitioning of fragment charges do not affect the results of the calculations but make them more readily interpretable.

The structures of the molecules studied were taken from those of the actual complexes $\text{FeFe}(1)$, $\text{CoCo}(2)$, $\text{NiNi}(3)$ and $\text{FeCo}(4)$ ^(3a,7), as well as $[(\eta^5\text{-C}_3\text{H}_5)\text{Co}(\mu, \eta^5\text{-C}_3\text{B}_2\text{R}_5)]_2\text{M}$ ($\text{M} = \text{Cr, Fe and Ni}$)⁽⁷⁾. The basis functions used for our calculation are listed in the Appendix. Occupations of the fragment orbitals, overlap populations and atomic charges were calculated by the Mulliken population analysis.

Acknowledgement: This research was supported in part by the computation centers at Heidelberg University and Nanjing University. L.Z. thanks Nanjing University, PRC, for leave of absence Oct.1987 – Apr. 1988, and August 1995. The work was supported by the Deutsche Forschungsgemeinschaft (SFB 247).

APPENDIX*

Fenske-Hall AO parameters

atom	function	coefficient	exponent
H	1s	1.0	1.2
C	1s	1.0	5.59
	2s	-0.22998	5.59
		1.0261	1.61
	2p	0.8017	1.2557
		0.26047	2.726
		0.9270	4.4456
B	1s	0.9270	4.4456
		0.0778	7.9180
		0.00088	0.8671
		-0.002	1.2192
		0.0043	2.0726
		0.0027	3.4433
	2s	-0.19484	4.4456
		-0.01254	7.9180
		0.06941	0.8671
		0.75234	1.2192
		0.31856	2.0726
		-0.12642	3.4433
	2p	0.53622	0.8748
		0.40340	1.3700
	0.11653	2.3226	
	0.00821	5.5948	
Cr	1s	1.0	23.39
	2s	-0.3624	23.39
		1.0636	8.9
	2p	1.0	9.7
	3s	0.1415	23.39
		-0.4792	8.9
		1.097	4.06
	3p	-0.3073	9.7
		1.0462	3.74
	3d	0.506	4.95
		0.675	1.8
	4s	-0.0556	23.39
		0.1926	8.9
		-0.5192	4.06
	1.1068	2.0	
Fe	1s	1.0	25.38
	2s	-0.3679	25.38
		1.0655	9.75
	2p	1.0	10.6
	3s	0.1455	25.38
		-0.4875	9.75
	3p	-0.3201	10.6
		1.05	4.17
	3d	0.5505	5.35
	0.626	2.0	

(continue)	atom	function	coefficient	exponent
	Fe	4s	-0.0469	25.38
			0.1605	9.75
			-0.4177	4.48
			1.0699	2.0
	Co	1s	1.0	26.375
		2s	-0.3704	26.375
			1.0664	10.175
		2p	1.0	11.05
		3s	0.1473	26.375
			-0.4912	10.175
			1.1012	4.69
		3p	-0.3256	11.05
			1.0517	4.385
		3d	0.5598	5.45
			0.6366	1.90
		4s	-0.05252	26.375
			0.1790	10.175
			-0.4683	4.69
			1.0870	2.2
		Ni	1s	1.0
	2s		-0.3727	27.37
			1.06720	10.60
	2p		1.0	11.50
	3s		0.1489	27.37
			-0.4945	10.60
			1.1024	4.9
	3p		-0.3308	11.50
			1.0533	4.60
	3d		0.5439	5.60
			0.6184	2.20
	4s		-0.03976	27.37
		0.1345	10.60	
		-0.3406	4.90	
		1.0468	2.0	

* 4p orbitals of Cr, Fe, Co and Ni atoms are deleted in our calculation because they have no significant contribution to bonding.

REFERENCE

- (1) (a) Werner, H., Salzer, A., *Inorg. Met.-Org. Chem.*, **2**, 239(1972).
 (b) Salzer, A., Werner, H., *Ibid.*, **2**, 249(1972).
 (c) Salzer, A., Werner, H., *Angew. Chem. Int. Ed. Engl.*, **24**, 949(1972).
- (2) Beer, D. C., Miller, V. R., Sneddon, L. G., Grimes, R. N., Mathew, M., Palcnik, G. J., *J. Am. Chem. Soc.*, **95**, 3046(1973).
- (3) (a) Edwin, J., Bochmann, M., Bohn, M. C., Brennan, D. E., Geiger, W. E., Krüger, C., Pebler, J., Pritzkow, H., Siebert, W., Swiridoff, W., Wadepohl, H., Weiss, J., Zenneck, U., *J. Am.*

Chem. Soc., **105**, 2582(1983).

- (b) Edwin, J., Bohm, M.C., Chester, N., Hoffman, D. M., Hoffmann, R., Pritzkow, H., Siebert, W., Stumpf, K., Wadepohl, H., *Organometallics*, **2**, 1666(1983).
- (c) Zwecker, J., Dissertation, Heidelberg, (1986).
- (d) Muhlfenzl, B., Dissertation, Heidelberg, (1985).
- (e) Wang, X., Sabat, M., Grimes, R.N., *J. Am. Chem. Soc.*, **116**, 2687(1994).
- (4) Lauher, J. W., Elian, M., Sumemerville, R. H., Hoffmann, R., *J. Am. Chem. Soc.*, **98**, 3219(1976).
- (5) (a) Chesky, P. T., Hall, M. B., *J. Am. Chem. Soc.*, **106**, 5168–5188(1984).
- (b) Li, Q. S., Yu, H. T., Tang, A. C., *Theor. Chim. Acta*, **70**, 379(1986).
- (c) Tang, A. C., Li, Q. S., *Int. J. Quantum. Chem.*, **29**, 579(1986).
- (d) Li, Q. S., Tang, A.C., *Acad. Sinica. (B. Section)*, **1**, 1(1989).
- (e) Tremel, W., Hoffmann, R., Kertesz, M., *J. Am. Chem. Soc.*, **111**, 2030(1989).
- (f) Hyla-Kryspin, I., Gleiter, R., Herberich, G. E., Benard, M., *Organometallics*, **13**, 1795(1994).
- (g) Jemmis, E. D., Reddy, A. C., *J. Am. Chem. Soc.*, **112**, 722(1990).
- (h) Jemmis, E. D., Reddy, A. C., *Prod. Indian Acad. Sci. (Chem. Sci.)*, **102**, 379(1990).
- (i) Jemmis, E.D., Reddy, A. C., Scherer, O. J., Winter, R., Heckmann, G., Wolmershauser, G., *Organometallics*, **11**, 3894(1992).
- (j) Jemmis, E. D., Reddy, A. C., *Organometallics*, **7**, 1561(1988).
- (6) Kudinov, A. R., Rybinskaya, M.I., Struchkov, Y. T., Yanovskii, A. I., Petrovskii, P.V., *J. of Organometal. Chem.*, **336**, 187(1987).
- (7) Wadepohl, H., Dissertation in Marburg, (1982).
- (8) (a) Maki, A. H., Berry, T. E., *J. Am. Chem. Soc.*, **87**, 4437(1965).
- (b) Prins, R., *Mol. Phys.*, **19**, 603(1970).
- (9) Schlafer, H.L., Gliemann, G., Basic Principles of Ligand Field Theory, Translated from the German by D. F Ilten., Wiley-Interscience, London, 1969.
- (10) Siebert, W., *Angew. Chem. Int. Ed. Engl.*, **24**, 943(1985).
- (11) Hall, M. B., Fenske, R. E., *Inorg. Chem.*, **11**, 768(1972).